# Analysis of the Rolling Phenomenon of a Reduced-Diameter Wheel for Freight Wagons, as a Function of Operating Factors

D. S. Pellicer[1,*] and E. Larrodé[2]

(1) University of Zaragoza,
María de Luna St., no. 4, 50018 Zaragoza, Spain.
(2) University of Zaragoza,
María de Luna St., no. 4, 50018 Zaragoza, Spain.

## 1    Introduction

The objective of this work is to tackle the wear problem for reduced-diameter wheels, which presumably do not undergo the same degradation as the ordinary-diameter wheels due to its greater angular contact with the rail. For that, a calculation model able to determine the life of a wheel as a function of operating factors, such as the nominal wheel diameter, is developed.

Nowadays, the needs in the field of logistics are changing and new transportation models are arising. One of the models that is becoming more popular in the last years is the rail motorway model, which consists in transporting whole freight articulated vehicles (road vehicles) on railway wagons (Jaro & Folgueira, 2012). Figure 1 shows a schematic diagram of this concept:



**Figure 1**. Rail motorway train ready for road vehicles (un)loading. Source: Own elaboration.

The adoption of this model often encounters the problem of loading gauge: Due to the height of the road vehicles (around 4 m), placing them on wagons leads to a further height increase over the rails that may conflict with the limits found in some tunnels or under some overpasses. One of the ways to reduce the total height is by using reduced-diameter wheels.

The process consists of defining a mathematical model under the behavioral equations extracted from the models that can explain wheel degradation, each of which includes a set of hypotheses. The analytical model should have to include as many influence factors as possible; however, the model size must be restricted for it to be computationally – efficient. That implies that additional hypotheses will be formulated in order to take out those factors with a lesser influence on wheel degradation.

The main contribution of this work consists in tackling the physical problem of wear for reduced-diameter wheels, which has been hardly treated due to the uniqueness of these wheels. Wheel, wheelset and bogie kinematics and dynamics have been studied in-depth, which makes the work insightful as it provides comprehension as to why wheel life depends on its diameter.

* Corresponding author dasapezu@unizar.es

# 2    Methods

This work follows a deductive method, as explained next:

First, the rail – wheel contact problem has been studied basing on the contact friction mechanics theory and the works and studies conducted from the second half of the 18th century.

Second, the contact models have been assessed regarding two criteria: accuracy and computational effort. Those with a higher accuracy and a lower computational cost have been chosen Hertz's solution, Polach's method, center of friction, energy transfer and fatigue index. For their application, the vehicle – track interface has been parametrized, which means that the factors involved in the said interaction have been assigned parameters.

Each of this models consists of a set of equations, which can be used to interrelate the models, so it is possible to construct a numerical analysis model in the form of an algorithm thanks to the existing links and adding new links (geometrical and other mathematical relations, for instance). This algorithm is programmed on mathematical equation solving software, which allows solving all of the equations after having inputted the data required by the models.

The algorithm output is the wear depth of each wheel on a bogie, but the appearing of RCF can be predicted as well. When the wear depth reaches a fixed limit on a wheel, then all of the bogie wheels are reprofiled with a lathe and the wear cycle starts over (the algorithm is run again).

Finally, the results for wheels of different diameter wheels are compared and conclusions upon their behavior and the diameter influence are drawn.

## 2.1    List of abbreviations

The abbreviations used in the rest of the article can be consulted in Table A1 for those with Latin symbols and Table A2 for those with Greek symbols (both in Annex 1).

## 2.2    Hypotheses

The following hypotheses have been regarded besides the application hypotheses of the models applied (Hertz's solution, Polach's method and center of friction model):
1. The procedure is based on global calculations for the contact patch, without discretizing it into finite elements.
2. It is stationary, that is, it does not consider the variation of variables over the time. At transition curves, where these variations are greater, mean values are computed.
3. It disregards any rail wear and it does not consider the previous wheel wear either (it does not update the contact parameters as the profile wears out, but this profile is assiduously renovated).

4. It is applied on all of the bogie wheels. For each wheel, the parameters and wear calculations are separately saved. This is because the wear is not the same for all of the wheels mounted on the same bogie (Rovira, 2012).
5. It is applied on one bogie belonging to a wagon. A wagon normally consists of two bogies, but they can mostly rotate independently with respect to the other.
6. It can consider up to 2 contact patches at the same wheel: one of them on the tread and the other on the flange. The load percentage of each patch will be controlled by means of a parameter (Pellicer & Larrodé, 2021).
7. Creepage is obtained from a kinematic analysis of the wheelsets rather than from the non-dimensional slips (these include partial derivatives which are usually not applied to global calculations).
8. In the whole study, the radial deformation $\delta_o$ is disregarded with respect to the wheel radius $r_o$ (this is a usual hypothesis in these studies because $\delta_o \ll r_o$).
9. As $\Phi \ll \gamma_o$ (in fact, $\Phi \ll \psi \ll \gamma_o$, judging by the values obtained in (Pellicer & Larrodé, 2021)), the effect of $\Phi$ on $\gamma_o$ can be disregarded as well.
10. In contrast, the effect of $\dot{\Phi}$ on the wear happening at transition curves is not considered, given that it increases the wear slightly.
11. Only abrasive and adhesive wear are considered, without considering defects such as cracks, spalling, squats, flats, etc. (Ortega, 2012), (RENFE, 2020).
12. RCF is only predicted, without computing the cracks generated (Ortega, 2012).
13. The bogie wheels are considered to be non-powered, so $F_t=0$ at the wheel-rail interfaces.
14. The bogie wheels are considered to be equipped with disk brakes, which do not wear the wheels out (Pellicer & Larrodé, 2021).
15. The railway vehicle is presumed to negotiate curves (circular or transition ones) at a constant speed, so it brakes (if necessary) before negotiating them, so $F_f=0$ at a curve.
16. The influence of manufacturing or assembly tolerances of any element is not considered.
17. By not considering rail deflection or manufacturing and assembly tolerances, it is possible to assume that the longitudinal rail curve radius ($R_{y,1}$) tends to infinity, so that the associated curvature ($1/R_{y,1}$) tends to zero and can be taken as such.

## 2.3  Calculation Process

An algorithm consisting of blocks has been constructed and is shown in Figure 2, where input data blocks are represented in green, intermediate equation blocks are in blue (light for kinematics and dark for dynamics) and the output blocks are in purple. The orange symbol with a diagonal cross represents the addition of values, the orange one with a Greek cross indicates a disjunctive, the gray one indicates that only one flow is inputted and the yellow a bifurcation:
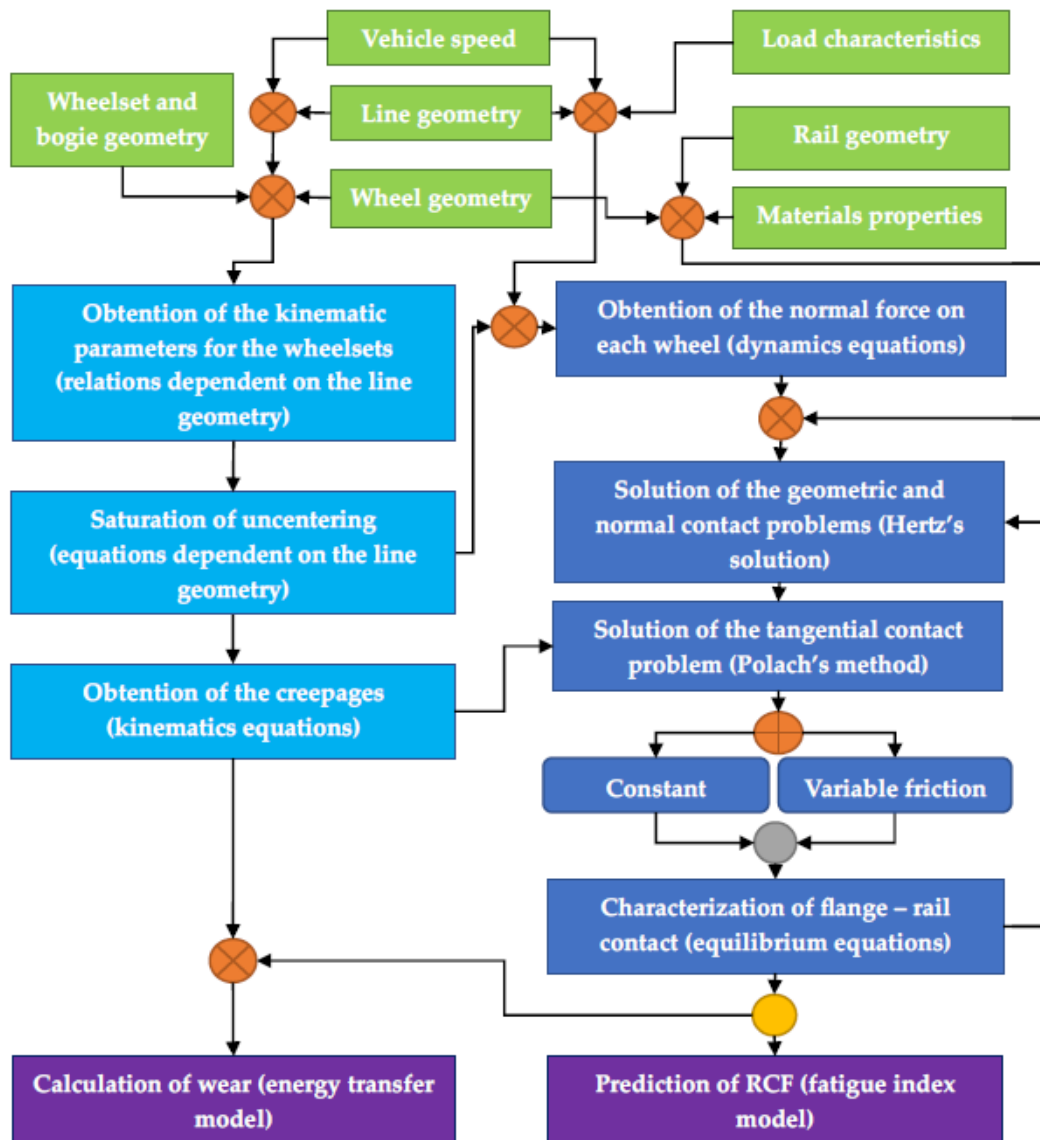
**Figure 2.** Flow diagram of the calculation process (algorithm). Source: Own elaboration.

## 2.4 Graphic description of the variables

First, four reference frames have been defined for the kinematics and dynamics analyses described in the next pages. These frames are described below and shown in Figure 3(a) for a wheelset (for the whole bogie does not need a specific reference frame):

- Absolute reference frame $XYZ$, clockwise, fixed on the rolling plane.
- Track reference frame $\tilde{x}\tilde{y}\tilde{z}$, clockwise, mobile at the vehicle speed, on the rolling plane.
- Axle reference frame $\bar{\bar{x}}\bar{\bar{y}}\bar{\bar{z}}$, clockwise, mobile at the axle speed, at the wheelset center.
- Contact area reference frame $x_c y_c z_c$, clockwise, mobile at the area speed, at its center.

These reference frames are mainly used for defining and placing and defining kinematic parameters (Figure 3(b)) and also contact patches and tangential forces at the wheels of a bogie (Figure 3(c)).

Finally, the elimination of wear by means of reprofiling is shown, which can be performed by reprofiling when its depth reaches a certain threshold (Alba, 2015):
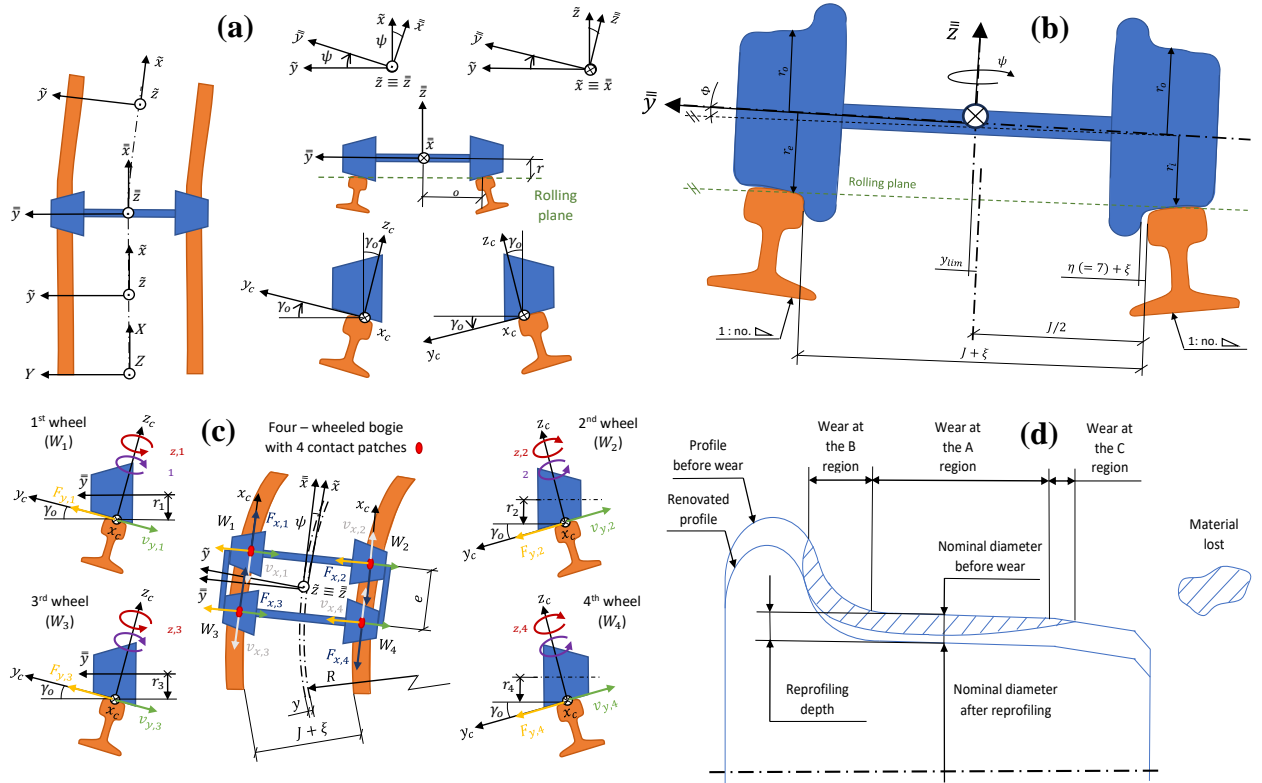
**Figure 3**. (**a**) Reference frames definition; (**b**) Wheelset positioning on a narrow curve where there is an uncentering limit imposed by geometrical constraints (for Iberian gauge, $J = 1668$ mm and $no. = 20$, so $\frac{J}{2} = 884$ mm); (**c**) Tangential forces and torques associated with the creepages at each wheel of a four-wheeled bogie; (**d**) Reprofiling of a wheel which has lost material to wear. Source: Own elaboration.

## 2.5 Kinematics equation blocks

References (Fissette, 2016), (Moody, 2014), (Oldknow, 2015), (Ortega, 2012), (Rovira, 2012) and (Sichani, 2016) explain how to obtain the kinematic parameters for the wheelsets through relations dependent on the railway line geometries; namely, straight stretch, circular curve and transition curve (clothoid, quadratic parabola or cubic parabola).

The parameters obtained at these geometries are described in Reference (Pellicer & Larrodé, 2021): uncentering and uncentering speed, average uncentering and uncentering speed, yaw angle and yaw angle variation speed / rate, average sinus of yaw angle and of yaw angle variation, average yaw angle, combination of the uncentering and yaw angle effects, angle of longitudinal displacement of the contact area, and, finally, tilt and tilt speed / rate.

As explained in References (Oldknow, 2015), (Ortega, 2012), (Rovira, 2012) and (Sichani, 2016), the total uncentering of a wheelset ($y^*$) can be computed by adding the original uncentering (($y$, which is the distance between the wheelset center of gravity and the track

center). The reason why uncentering must be saturated is because there exists a geometrical constraint: the flange (the flange enters in contact with the rail).

As to the creepages, they are the rigid slip velocities divided by the vehicle speed in order to turn them into non-dimensional. References (Fissette, 2016), (Ortega, 2012), (Pellicer & Larrodé, 2021) and (Sichani, 2016) explain how to compute them from kinematics parameters:

1. Longitudinal creepage: Difference between the nominal wheel radius and the real rolling one (generates $V_x^I$), application of tractive or braking torques to the wheel ($V_x^{II}$) and variation of yaw angle ($V_x^{III}$).
2. Transversal creepage: Not null yaw angle ($\Delta V_y^I$), adoption of a new equilibrium position by the wheelset ($\Delta V_y^{II}$) and not null tilt angle ($\Delta V_y^{III}$).
3. Spin: Conicity ($\Delta \Phi^I$; "camber effect") and variation of yaw angle ($\Delta \Phi^{II}$).

Finally, the main kinematics equations are shown: uncentering (1), its saturation (2 − 5), creepages definition (6 − 8), longitudinal creepage (9 − 11), transversal creepage (12 − 14) and spin (15 − 17):

$$y = \frac{r_o b_o}{kR} \qquad (1)$$

$$y^* \ (1^{st} \ wheelset) = y + e\frac{\pi \ |\psi|}{360} \qquad (2)$$

$$y^* \ (2^{nd} \ wheelset) = y - e\frac{\pi \ |\psi|}{360} \qquad (3)$$

$$y_{lim}^* = \frac{\eta}{2} + \xi \qquad (4)$$

$$y^* = y_{lim}^* \ (\text{if the former was greater before}) \qquad (5)$$

$$v_x = \Delta V_x / V \qquad (6)$$
$$v_y = \Delta V_y / V \qquad (7)$$

$$\varphi = \Phi / V \qquad (8)$$

$$\Delta V_x = V_x^I + V_x^{III} + V_x^{III} \qquad (9)$$

$$\Delta V_x = -\Delta r \ \omega - r_o \omega' \pm b_o \dot\psi \qquad (10)$$

$$v_x = \frac{-\Delta r}{r_o} + \frac{-r_o \omega' \pm b_o \dot\psi}{V} \qquad (11)$$

$$\Delta V_y = V_y^I + V_y^{III} + V_y^{III} \qquad (12)$$

$$\Delta V_y = -V sen\psi \ cos\gamma_o + \dot y \cos \gamma_o - r_i \dot\Phi \cos \gamma_o \qquad (13)$$

$$v_y = \left(-sen\psi + \frac{\dot y - r_i \Phi}{V}\right) cos\gamma_o \qquad (14)$$

$$\Delta \Phi = \Delta \Phi^I + \Delta \Phi^{II} \qquad (15)$$

$$\Delta \Phi = \pm \omega \ sen\gamma_o + \dot\psi \cos \gamma_o \qquad (16)$$

$$= \pm \frac{sen \ \gamma_o}{r_o} + \frac{\dot\psi \ cos\gamma_o}{V} \qquad (17)$$

## 2.6  Dynamics equation blocks

The normal force is exerted by the rail on the wheel as a response to the opposite force the latter exerts on the former. References (ADIF, 1983 − 2021), (Andrews, 1986), (Fissette, 2016), (Moody, 2014), (Rovira, 2012), (Tipler & Mosca, 2014) provide some information on how to compute the normal force on each wheel. However, the most important Reference is (Pellicer & Larrodé, 2021), as it is the one which fills the gaps and obtains the normal force on each wheel as a function of these factors: axle load ($\lambda_{eje}$), center of gravity of the axle load ($H_{CdG}$), gradient angle ($\beta_{rp}$) inferred from the inclination ($i$), cant angle ($\vartheta_r$), lateral acceleration ($a_{lat}$), which considers the effect of cant excess of deficiency, and, finally, wheel contact angle ($\gamma_o$) and longitudinal displacement angle of the contact patch ($\varsigma$). This allows computing the normal

force on the external and internal wheel to a curve ($N_e$ and $N_i$, respectively) and decomposing it in their perpendicular and parallel components ($N_\perp$ and $N_\parallel$).

On the other hand, an isolated wheel transmits its own weight and its load to the rail, with which is shares an interface: the contact area. The contact area must be greater than zero in order to avoid an infinite normal stress. Both the contact area (geometry problem) and the normal stress must be determined so as to compute the wear and know where it acts (normal problem). As explained in Reference (Sichani, 2016), whenever two bodies make contact, that contact can be non-conformal or conformal. In the former, the contact area is relatively small in comparison with the characteristic size of the bodies; while in the latter, the geometry of a body adapts to the geometry of the other, resulting in a relatively big contact area (happening when the wheel and rail are heavily worn-out). Conformal contacts can be further simplified if the quasi-identity relation is fulfilled, which means that a relation between the shear modulus and the Poisson's ratio exists; this condition is fulfilled because the materials in contact are the same (steel).

Both the geometric and the normal contact problem are solved together, and in References (Ortega, 2012), (Rovira, 2012) and (Sichani, 2016), some theories for solving them are commented upon. As stated in Reference (Pellicer & Larrodé, 2021), which collects the theories, the Herztian contact theory is the most common due to its high accuracy, low computing effort and because the hypotheses it brings are fulfilled for most of the cases:
- The bodies in contact are homogeneous, isotropic and linear elastic.
- Displacements are supposed to be infinitesimal (much smaller than the bodies' characteristic dimensions).
- The bodies are smooth at the contact zone, that is, without any roughness.
- Each body can be modeled as an elastic half-space, which requires non-conformity.
- The bodies' surfaces can be approximated by quadratic functions in the vicinity of the maximum interpenetration point. This implies that the curvatures (the second derivates of the functions) are constant.
- The distance between the undeformed profiles of both bodies at the maximum interpenetration point can be approximated by a paraboloid.
- The contact between the bodies is made without friction, so only normal pressure can be transmitted.

Nonetheless, the Hertzian model ignores the forces and torques due to friction: as a consequence of the relative motion between the wheel and the rail in the longitudinal and lateral directions and around the vertical axis ($z_c$), opposing forces and torques appear. These are associated with tangential stresses and deformations at the contact area, specifically at the slip region of the ellipse (split into one stick and one slip region). There are two ways to compute these variables:
- Analytical way: The values are globally computed for the whole contact patch. A set of analytical equations are used, and the tangential problem can be decoupled from the geometric and normal ones because non-conformity and quasi-identity are satisfied.
- Finite-element way: The values of the variables are locally computed and are added thereafter so as to obtain the global values. For that, the contact patch is meshed.

In the current work, the analytical way is chosen, inasmuch as that it allows tackling the problem with an algorithm which comes to the results at a good accuracy – computational effort ratio. For the computation of these tangential forces and also the spin torque, in References (Rovira, 2012), (Sichani, 2016) and (Ortega, 2012) some models are commented upon. Reference (Pellicer & Larrodé, 2021) collects them, concluding that Polach's method is the most appropriate for considering the spin effect, since it brings accurate results with a low effort.

So as to find the reaction that the rail exerts on the flange when they enter in contact, Reference (Andrews, 1986) proposes the center of friction model. This model states that every bogie, when curving, has a point at which, if a wheel were mounted there, this wheel would spin ideally, that is, with no slip. This point is called the center of friction and determining it allows computing the forces exerted by the rail on the flange – rail contact through force and torque balances.

As for the load distribution on each contact, Reference (Piotrowski & Chollet, 2005) explains the Sauvage model, a heuristic method to obtain the total indentation ($\delta_o$) as the sum of the indentation at the tread – rail contact ($\delta_{br}$) and that at the flange – rail contact ($\delta_{pe}$). Reference (Pellicer & Larrodé, 2021) simplifies the Sauvage model by introducing the load distribution coefficient ($\alpha_{fn}$), ranging from 0.5 (same normal load for both contacts) and 1 (the tread contact would become discharged). Its usual values are taken from the results of the Sauvage model: 0.7 – 0.8. At the end, this method is combined with the center of friction one.

Finally, the dynamics equations are presented: Eqs. 18 – 26 allow computing the normal force on each wheel (Larrodé & Pellicer, 2021), Eqs. 27 – 36 allow applying Hertz's solution (Greenwood, 2018), (Hertz, 1882), Eqs. 37 – 46 allow applying Polach's method (Polach, 2000), (Polach, 2005) and, finally, Eqs. 47 – 51 allow applying the center of friction model:

$$\lambda_{eje} = \frac{\lambda_u + \lambda_{tara}}{n_{ejes}} \tag{18}$$

$$p_{z_o} = \frac{3F_z}{2\pi ab} \tag{35}$$

$$H_{CdG} = \frac{\frac{1}{n_{ejes}}(\lambda_u H_u + \lambda_{tara} H_{tara})}{\frac{1}{n_{ejes}}(\lambda_u + \lambda_{tara})} \tag{19}$$

$$\delta_o = r_H \left( \left( \frac{3}{2} N \frac{1-v^2}{E} \right)^2 (A + B) \right)^{\frac{1}{3}} \tag{36}$$

$$\beta_{rp} = arctan\left(\frac{i}{1000}\right) \tag{20}$$

$$s_i = \frac{\mu N_\perp}{Gab\, C_{jj}} v_i, \quad i,j = x,1; \ i,j = y,2 \tag{37}$$

$$\vartheta_r = arcsen\left(\frac{h_r}{2b_o}\right) \tag{21}$$

$$s_{y,C} = s_y + (-\varphi)a, \qquad |s_y + (-\varphi)a| > |s_y| \tag{38}$$

$$a_{lat} = \frac{v^2}{R+y} - \frac{h_r'}{2b_o} g \cos\beta_r \tag{22}$$

$$s_{y,C} = s_y, \qquad\qquad |s_y + (-\varphi)a| \leq |s_y| \tag{39}$$

$$N_e = \frac{\lambda_{eje}}{2}\left(1 + \frac{y}{b_o}\right) g \cos\vartheta_r \cos\beta_{rp} + \frac{\lambda_{eje}}{2b_o} a_{lat} H_{CdG} \tag{23}$$

$$F = -\frac{2\mu N_\perp}{\pi}\left(\frac{\varepsilon}{1+\varepsilon^2} + arctan\varepsilon\right) \tag{40}$$

$$N_i = \frac{\lambda_{eje}}{2}\left(1 - \frac{y}{b_o}\right) g \cos\vartheta_r \cos\beta_{rp} - \frac{\lambda_{eje}}{2b_o} a_{lat} H_{CdG} \tag{24}$$

$$F_i = F \frac{s_i}{s}, \qquad i = x,y \tag{41}$$

$$N_\perp = N_{e|i} \cos(\varsigma) \cos(\gamma_o) \tag{25}$$

$$F_{y,S} = -\frac{9}{16} a\, \mu N_\perp\, K_M \left[1 + 6{,}3\left(1 - e^{-\frac{a}{b}}\right)\right]\frac{(-\varphi)}{s_C} \tag{42}$$

$$N_\parallel = N_{e|i} \cos(\varsigma) \sin(\gamma_o) \tag{26}$$

$$F_{y,C} = F_y + F_{y,S} \tag{43}$$

$$A = \frac{1}{2}\left(\frac{1}{R_{y_1}} + \frac{1}{R_{y_2}}\right) \tag{27}$$

$$F = -\frac{2\mu N_\perp}{\pi}\left(\frac{k_A \varepsilon}{1+(k_A \varepsilon)^2} + arctan(k_S \varepsilon)\right) \tag{44}$$

$$B = \frac{1}{2}\left(\frac{1}{R_{x_1}} + \frac{1}{R_{x_2}}\right) \qquad (28)$$

$$R_{y_2} = \frac{r}{cos\gamma_o} \qquad (29)$$

$$A_c = \pi a b \qquad (30)$$

$$a = m_H \left(\frac{3}{2} N \frac{1-v^2}{E} \frac{1}{A+B}\right)^{\frac{1}{3}} \qquad (31)$$

$$= n_H \left(\frac{3}{2} N \frac{1-v^2}{E} \frac{1}{A+B}\right)^{\frac{1}{3}} \qquad (32)$$

$$\frac{1-v^2}{E} = \frac{1}{2}\left(\frac{1-v_1^2}{E_1} + \frac{1-v_2^2}{E_2}\right) \qquad (33)$$

$$cos\theta = \frac{|B-A|}{A+B} \qquad (34)$$

$$\mu = \mu_o\left[(1 - A_f)e^{-wB_f} + A_f\right] \qquad (45)$$

$$w_i = s_i V \qquad i = x, y \qquad (46)$$

$$\zeta_v = \alpha_{fn} N_e \qquad (47)$$

$$N_p = \zeta_v \, cos\gamma_o + \zeta_h \, sen\gamma_o \qquad (48)$$

$$(-F_t|+F_f) = -\sum_{i=1}^{i=Z_w+2} F'_{x,i} \qquad (49)$$

$$\zeta_{h,1} - \zeta_{h,Z_w} = \sum_{i=1}^{i=Z_w+2} F'_{y,i} \qquad (50)$$

$$\zeta_{h,1} u_{fl,1} - \zeta_{h,Z_w} u_{fl,4} = \sum_{i=1}^{i=Z_w+2}\left(F'_{y,i} \, u_{f,i}\right) + \\ + \sum_{i=1}^{i=Z_w+2}\left(F'_{x,i} \, v_{f,i}\right) \qquad (51)$$

## 2.7 Calculation of wear and prediction of RCF

Abrasive wear is due to the relative movement between the wheel and rail surfaces and their roughness, which cause friction and this, in turn, the loss of wheel and rail material. In contrast, adhesive wear is due to plastic deformation and to the cohesive forces appearing between both surfaces (Van der Waals, electrostatic or chemical), which ends up producing a material transfer from one surface to the other (Rovira, 2012). For wheel wear characterization, the same Reference listed the following hypotheses:

1. The equations are parametrized for abrasive wear and not for adhesive wear because: (both phenomena are included in the resulting wear law if experimentally calibrated).
2. The different mathematical tools study the wear on the wheel profile, where the wear estimated at every instant is cumulative.
3. Wear is assumed to be regular: the variation of the transversal profile is studied, not pattern formation along the longitudinal (circumferential) direction. Thus, the wear at a certain position and instant is extrapolated to the whole circumference.
4. At the contact interface there are not any pollutants. The effect of pollutants is considering by modifying the friction coefficient or introducing new wear laws.

Considering these hypotheses, the models commented upon in References (Rovira, 2012) and (Sichani, 2016) can be applied to wheel wear characterization. In Reference (Pellicer & Larrodé, 2021), energy transfer models and the RAK model are collected and assessed and it was determined that the energy transfer using the USFD wear law since its wear law is continuous, so small errors do not lead to great errors in the end.

Under high axle loads, the stress distribution around the contact patch may cause fatigue cracks on the wheel surface or inside it. For only predicting if RCF is to appear or not, the fatigue index model developed by Reference (Dirks, Ekberg & Berg, 2015) and presented in Reference (Sichani, 2016) is useful. The fatigue index ($FI_{suf}$) is simply the utilized friction term ($\mu_u$) minus the shakedown limit ($L_{RCF}$) and by comparing its value with zero, 3 situations can be observed: if $FI_{suf} < 0$, RCF is not enough for initiating cracks, while if $FI_{suf} = 0$, this is the limit situation and cracks are not initiated yet. However, if $FI_{suf} > 0$, RCF initiates cracks on the surface since the tangential force is elevated.

Finally, the main equations of the USFD law (52 – 56) and the fatigue index model (57 – 59) are presented:

$$\frac{T\gamma}{A_c} = \frac{|F_x v_x| + |F_y v_y| + |M_z \varphi|}{A_c} \quad (52)$$

$$H_{USFD} = W_{R,USFD} \frac{a\,L_{rr}}{\rho \pi r_{rr}} 10 \quad (56)$$

$$W_{R,USFD} = 5.3\,\frac{T\gamma}{A_c}, for\,\frac{T\gamma}{A_c} \le 10.4 \quad (53)$$

$$FI_{surf} = \mu_u - L_{RCF} \quad (57)$$

$$W_{R,USFD} = 55.0, for\,10.4 < \frac{T\gamma}{A_c} \le 77.2 \quad (54)$$

$$FI_{surf} = \frac{\sqrt{F_x^2 + F_y^2}}{N} - \frac{\tau_{lim}}{p_{z_o}} \quad (58)$$

$$W_{R,USFD} = 55.0 + 61.9\left(\frac{T\gamma}{A_c} - 77.2\right), for\,\frac{T\gamma}{A_c} > 77.2 \quad (55)$$

$$F_{max,RCF} = \frac{2}{3}\tau_{lim}\pi ab \quad (59)$$

## 2.8 Software Choice

Once the algorithm architecture and details have been defined, it must be implemented in an equation solving program. Due to the large number of input data, equations, relations, functions, procedures and subroutines which had to be implemented, only software capable of processing the entire volume of data in an agile way has been considered. After considering several options (Mathematica, Matlab and Engineering Equation Solver), Engineering Equation Solver (Klein, 1993) has been chosen, as it is a program which allows building algorithms with any architecture, basing on functions, procedures and subroutines defined in F-Chart programming language, which is a variation of Pascal. The program rearranges internally the equations blocks defined by the user, takes the inputs needed for the new blocks and obtains the requested outputs by means of iterations. These results are obtained after an undetermined number of iterations, depending on adjustable stop criteria such as the relative residuals, which can be as low as $10^{-10}$, or the limit of iterations. The specific version with which the results were obtained is Engineering Equation Solver Professional V9.457-3D (EES). The chosen program, besides solving algorithms, can create parametric tables and graphs derived from those equations.

## 2.9 Calculation Scenarios

The objective is to calculate the wear as a function of operating factors such as the nominal diameter for various wheels and compare the results. For the comparison, these commercial bogies, used or proposed on rail motorways, have been chosen:
- Y – 25: This bogie consists of four wheels (thus, it is composed of two wheelsets) and it can take up 45 t in total (22.5 t/axle) at a maximum speed of 120 km/h. The axle span ($e$) is variable and the wheels are braked, in general, by brake shoes. The wheel nominal diameter ($D$) ranges from 920 mm (original) to 840 mm (operational minimum).
- Saas-z 703: This bogie also consists of four wheels (so two wheelsets) and it can take up 32 t (16 t/axle) at 100 km/h. The axle span ($e$) is variable and the wheels are braked by brake disks. The wheel nominal diameter ($D$) ranges from 680 mm to 630 mm.

- Graz Pauker 702: This bogie is composed of eight wheels (so four wheelsets) and it can withstand 20 t (5 t/axle) at 100 km/h. The axle span ($e$) is variable and the wheel nominal diameter ($D$) ranges from 355 to 335 mm.

These bogies are different each other, but the comparisons should be performed under the same conditions (only excluding the nominal diameter variation), yet comparing the scenarios under the same conditions is not always possible, as stated in Reference (Pellicer & Larrodé, 2021):

1. Axle load ($\lambda_{eje}$): If a constant axle load value were given for all of the cases, then the wheels would be overloaded in some scenarios, while underloaded in others. On the one hand, some values as high as 22.5 t/axle would be unrealistic and unfeasible for the 680 and 355-mm wheels. On the other hand, some values as low as 5 t/axle would be realistic and feasible, although the smallest wheel (355 mm) would be fully loaded, working at maximum normal pressure and tangential stresses at the tread – rail interface, while the biggest wheel (920 mm) would be barely loaded, working at low values of those variables. In order to ensure (as much as possible) the same conditions, the axle load generating the same normal pressure is to be chosen. Specifically, the axle load generating a 1,235 MPa normal pressure.

2. Flange radius ($r_p$): It is the addition of the nominal rolling radius ($r_o$, which is a half of $D$) and a constant. So $r_p$ decreases in proportion with $D$.

The rest of conditions are the same (for instance, the axle span) and are discussed in the Input data section. Only realistic, feasible and plausible values are set and even variations in the geometry and friction are considered (the variation of dry friction with speed).

Taking all of this into account, the three scenarios are established: 920-mm, 680-mm and 355-mm wheels. For each of them, the input data is entered at first, and then the program runs the algorithm for every stretch of the railway line, switching the direction when the end station is reached. When the wear depth reaches a certain threshold (1 mm in this case, a low value as the wheel profiles are not steadily updated), then the wheel is reprofiled and the scenario execution starts over with a new wheel profile (with a lesser diameter now). After a certain number of reprofiling cycles is reached, the minimum allowed diameter is reached, and the scenario execution ends. All of this leads to the results: the wheel diameter – mileage curves.

## 2.10  Input Data

For the three scenarios, the wheel profile portrays the geometry of the 1/40 standard profile and is made from ER8 steel grade, while the rail profile portrays the geometry of the 60E1 standard profile and is made from R260 steel grade (AENOR, 2011 – 2021). Most of the wheelset and bogie characteristics, which are taken from the bogie comparison carried out in Reference (Pellicer & Larrodé, 2021) are also common to the three scenarios. The same for the parameters used to modify friction with speed according to Polach's method (implemented with variable friction under dry conditions). These common input data are shown in Table A3 (Annex 1).

However, some features as the diameter, number of axles, axle load and flange radius are not common and depend on the scenario. These scenario-dependent are discussed in Reference (Pellicer & Larrodé, 2021) and are displayed in Table A4 (Annex 1).

As for the railway line parameters, the calculation is performed for the three scenarios with data from a non-existing railway line. The design parameters of a railway line are defined in References (ADIF, 1983 – 2021) and (Vera, 2016), although not all of the parameters are used for wear calculation. In Reference (Pellicer & Larrodé, 2021), a railway line is defined stretch by stretch, with these parameters: initial and final metric points ($Q_{in}$ and $Q_f$); type of stretch: RECTA (straight), CIR (circular curve), CLO (clothoid), PARACUAD (quadratic parabola) or PARACUB (cubic parabola); direction of the curve: NING (straight stretch), IZDA (curve to the left) or DCHA (curve to the right); position of the bogie at the curve: NING (straight stretch), ENT (bogie entering the curve), SAL (bogie exiting the curve); curve radius ($R$), cant ($h_r$) and inclination ($i$); and, finally, initial and final maximum speed allowed ($V_{in}$ and $V_{fn}$).

In the supplementary material (Pellicer & Larrodé, 2024), the 333 stretches defined can be found. It can be noted that 200 – 800-m radii are the most frequent, and because $\infty$ is not accepted on EES, it is assimilated to $5 \cdot 10^7$. For more realism, the station 1 is called Albarque, the station 2 is called Zacarín and there is even an intermediate station called Milbello (all of these are fictional names). The supplementary material also includes the introduction strategy of Hertz's and Kalker's coefficients into the analysis through polynomials and other equations.


# 3 Results

After executing the algorithm, the diameter – mileage curves are obtainer. Here, the diameter is expressed in [mm], whereas the distance traveled is in [km]. The results, shown in Figure 4, are briefly commented upon:

1. 920-mm wheels can travel for 115,476 km until reaching an 840-mm, losing 2 mm in diameter at every reprofiling cycle. However, if the train operator releases the 840-mm wheel from the workshop, the distance traveled will be augmented to 119,551 km. At that point, the worn-out profile will be discarded for safety and operational reasons.
2. 680-mm wheels are able to travel for 91,368 km until reaching their minimum allowed diameter: 620 mm. This is the real life end for this wheel, yet the wear – reprofiling cycles have been extended, as if the final diameter could be 600 mm for the difference between 680 and 600 is the same as that of 920 and 840. In this fictional situation, the wheel would have traveled 120,667 km (fictional life end).
3. 355-mm wheels are capable of traveling 35,311 km until reaching their minimum allowed diameter: 335 mm. This is the real life end for this wheel, yet the wear – reprofiling cycles have been extended, as if the final diameter could be 275 mm for the different between 355 and 275 is the same as that of 920 and 840. In this fictional situation, the wheel would have traveled 133,340 km (fictional life end).

Besides, a worn-out wheel profile after a random distance is obtained and represented with the coordinates $z_{p,f} - y_{p,f}$ ($z_{p,f}$ is the vertical coordinate of the final profile, while $y_{p,f}$ is the horizontal one). The profile shows that the flange wear is far more noticeable and significant than the almost-negligible tread wear (it is an aggressive type of contact and tight curves are predominant in the railway line defined). In fact, the algorithm determines that in most flange – rail contacts, RCF appears due to the high normal pressures and tangential stresses involved:
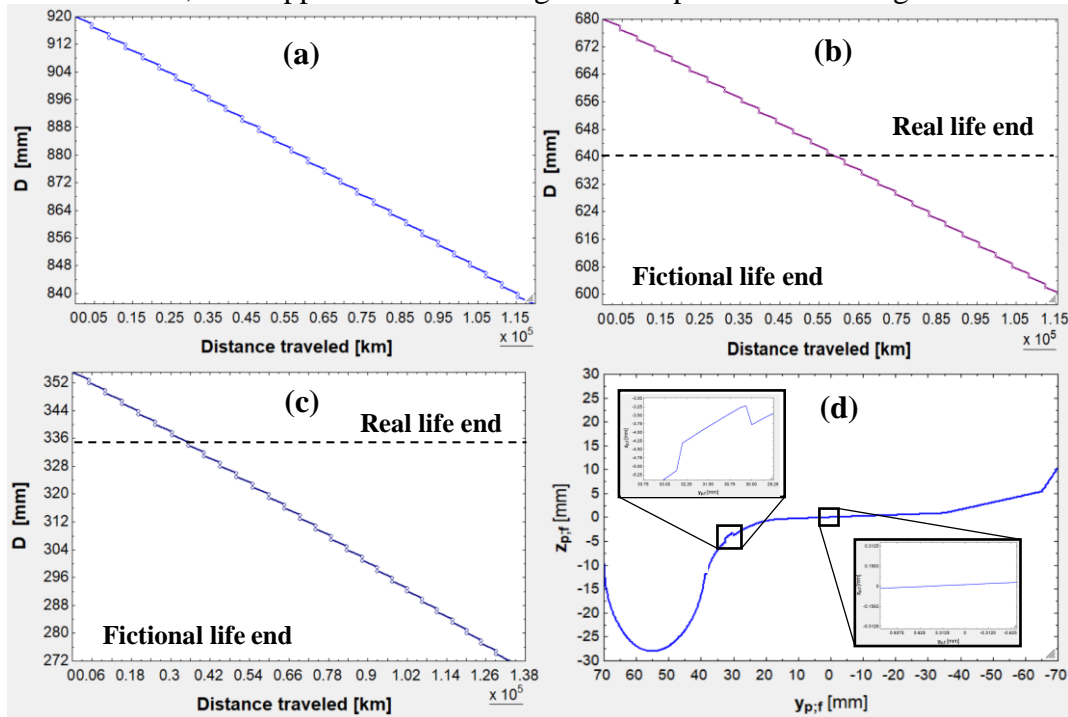


**Figure 4.** (**a**) Diameter – mileage curve for the 920-mm scenario; (**b**) Diameter – mileage curve for the 680-mm scenario; (**c**) Diameter – mileage curve for the 355-mm scenario; (**d**) Representation of a worn-out wheel profile after a random distance traveled.

## 4    Conclusions

The algorithm constructed interconnects some calculation models by other authors, all of which exhibit good accuracy – computational effort ratios. Moreover, it allows taking into account the main factors impacting wheel wear, some of which are associated with the vehicle (wheel and wagon factors), while others are associated with the superstructure. By introducing boundary conditions and hypothesis complementing those of the calculation models used, the algorithm enables computing the wear with a parametric variation (diameter variation, among others).

In the case presented, wheel wear computations have been utilized for the obtention of diameter – mileage curves for several scenarios: 920-mm diameter wheels used on the $Y - 25$ bogie, 680-mm diameter wheels used on the Saas-z 702 bogie and 355-mm diameter wheels used on the Graz Pauker 702 bogie. According to the results, smaller wheels can travel shorter than bigger

wheels as it was expected. However, this is due to the limit of reprofiling cycles and, as it has been discussed, if all of the wheels could undergo the same number of reprofiling cycles, then 680-mm diameter wheels could travel longer than 920-mm diameter wheels and 355-mm wheels could travel longer than its bigger counterparts. Despite being unexpected, the comprehension of wheel, wheelset and bogie kinematics and dynamics which this work has enabled, allows finding the root causes responsible for this behavior:

1. Regarding kinematics, reduced-diameter wheels negotiate curves more smoothly than ordinary-diameter wheels, as their uncentering is lower, so their flanges touch the rails less frequently (the threshold radius is lower as well).
2. Regarding dynamics, flange – rail contact is softer. When reduced-diameter wheels' flanges touch the rails, they do it less intensely (uncentering forces are not so intense). Also, the force exerted by the rails on the flange is lower because the bogies based on reduced-diameter wheels are less loaded, so the force and torque balances lead to lower rail – flange forces.

Finally, as a continuation of this research work, the variation of other parameters different to wheel diameter could be implemented in order to develop sensitivity analyses with the goals of optimization or finding and explaining trends.

## Acknowledgements

## References

[1] ADIF. Calificación, geometría, montaje y diseño de la vía. 1983 – 2021.

[2] AENOR. Aplicaciones ferroviarias. Ruedas y carriles. 2011 – 2021.

[3] Alba, M. V. Optimización de la Política de Reperfilado de Ruedas para el Citadis 302, en la explotación de Metro Ligero Oeste. *Revista Vía Libre Técnica, 9*, 29 – 38, 2015.

[4] Andrews, H. I. Railway Traction. The Principles of Mechanical and Electrical Railway Traction, 1st ed.; ElSevier Science*:* Oxford, 1986.

[5] Dirks, B.; Enblom, R.; Ekberg, A.; Berg, M. The development of a crack propagation model for railway wheels and rails. *Fatigue & Fracture of Engineering Materials & Structures*, *18(12)*, 1478 – 1491, 2015.

[6] Fissette, P. Railway vehicle dynamics. Teaching content. Catholic University of Louvain, Louvain. 2016.

[7] Greenwood, J. A. Hertz theory and Carlson elliptic integrals, *Journal of the Mechanics and Physics of Solids*, 119, 240 – 249, 2018.

[8] Hertz, H. R. Über die Berührung fester elastische Körper. *Journal für die reine und angewandte Mathematik 92,* 156 – 171, 1882.

[9] Jaro, L.; Folgueira, C. A. Las Autopistas ferroviarias: ¿Una apuesta de futuro en líneas mixtas de alta velocidad? *Revista de Alta Velocidad*, 2, 73 – 96, 2012.

[10] Kalker, J. J. Rolling contact phenomena - linear elasticity, *CISM International Centre for Mechanical Sciences*, 411th ed.*;* Springer: Vienna, Austria, 2000.

[11] Klein, S.A. Development and integration of an equation-solving program for engineering thermodynamics courses. *Computer Applications in Engineering Education, 1(3)*, 265–275, 1998.

[12] Larrodé, E. *Ferrocarriles y tracción eléctrica*, 1st ed.; Editorial Copy Center: Zaragoza, España, 2007.

[13] Moody, J. C. Critical Speed Analysis of Railcars and Wheelsets on Curved and Straight Track. Bachelor's Thesis. Bates College, Lewison, USA, 2014.

[14] Oldknow, K. Wheel – Rail Interaction Fundamentals. Course content. 2015.

[15] Ortega, E. Simulación del contacto rueda – carril con Pro/ENGINEER, Bachelor's Thesis, Universidad Carlos III, Madrid, España, 2012.

[16] Pellicer, D. S.; Larrodé, E. Analysis of the rolling phenomenon of a reduced-diameter railway wheel for freight wagons, as a function of operating factors. Master's Thesis, University of Zaragoza, Zaragoza, Spain, 2021.

[17] Pellicer, D. S.; Larrodé, E. Supplementary material of "Analysis of the rolling phenomenon of a reduced-diameter railway wheel for freight wagons, as a function of operating factors". *Mendeley Data,* 2nd version*,* 2024.

[18] Piotrowski, J.; Chollet, H. Wheel – rail contact models for vehicle system dynamics including multi-point contact. *Vehicle System Dynamics*, 43(6 – 7), 455 – 483, 2005.

[19] Polach, O. A Fast Wheel – Rail Forces Calculation Computer Code. *Vehicle System Dynamics*, *33(1)*, 728 – 739, 2000.

[20] Polach, O. Creep forces in simulations of traction vehicles running on adhesion limit. *Wear, 258(7 – 8), 992 – 1000, 2005.*

[21] Rovira, A. Modelado del contacto rueda-carril para aplicaciones de simulación de vehículos ferroviarios y estimación del desgaste en el rango de baja frecuencia. PhD Thesis, Polytechnical University of Valencia, Valencia, Spain, 2012.

[22] Sichani, M. S. On Efficient Modelling of Wheel – Rail Contact in Vehicle Dynamics Simulation. PhD Thesis, KTH Institute of Technology, Stockholm, 2016.

[23] Tipler, P. A.; Mosca, G. *Physics for Scientists and Engineers Vol. I,* 6th ed.; Macmillan Education: London, UK, 2014.

[24] Vera, C. Proyecto Constructivo de una Línea Ferroviaria de Transporte de Mercancías y su Conexión a la Red Principal. Bachelor's Thesis, University of Seville, Seville, Spain, 2015.

## Annex 1

**Table A1.** Latin-symbol abbreviations.

| Abbreviation | Definition | Unit (SI) | Abbreviation | Definition | Unit (SI) |
|---|---|---|---|---|---|
| $a$ | Longitudinal semi-axis of Hertz's ellipse | m | $n_{dec}$ | Degree of the function deceleration - time | ∅ |
| $a_{lat}$ | Lateral acceleration experienced by the vehicle | $m \cdot s^{-2}$ | $n_{ejes}$ | Number of axles on the vehicle | ∅ |
| $A$ | Relative longitudinal curvature | $m^{-1}$ | $n'_{ejes}$ | Number of axles on the bogie | ∅ |
| $A_c$ | Hertz's ellipse area | $m^2$ | $n_H$ | Lateral Hertz's coefficient | ∅ |
| $A_f$ | Ratio between the minimum friction coefficient (infinite slip speed) and the maximum (null slip) | ∅ | $N_{br}\|N_p$ | Reaction force of the rail on the wheel in the normal direction to the contact area at the (tread flange) at a wheel experiencing flange – rail contact | N |
| | Lateral semi-axis of Hertz's ellipse | m | $N_e\|N_i$ | Normal force acting on the (external ǀ internal) wheel to the curve | N |
| $b_i\|b_e$ | Distance from track center to the rolling radius of the (internal ǀ external) wheel to the curve | m | $N_r\|N_t$ | Normal force component in the radial ǀtangential direction (the tangential one is perpendicular to the radial one) | N |
| $_o$ | Distance from track center to rolling radius | m | $N_\perp\|N_\parallel$ | Normal force component acting on the wheel (perpendicularly ǀ tangentially) to contact area | N |
| $B$ | Relative lateral curvature | $m^{-1}$ | $o$ | Existing offset between the track gauge minus the flange – rail play and the distance between the nominal radius center of the wheelset wheels | m |
| $B_f$ | Exponential constant at friction law | $s \cdot m^{-1}$ | $p_{z_o}$ | Maximum contact normal pressure | Pa |
| $c$ | Effective size of contact patch | m | $Q_i\|Q_f$ | Initial ǀ final metric point | m |
| $C$ | Contact tangential stiffness | $N \cdot m^-$ | $r_e\|r_i$ | Theorical rolling radius of the (external ǀ internal) wheel to the curve | m |
| $C_s$ | Contact tangential stiffness for the pure spin case | $N \cdot m^-$ | $r_e^*\|r_i^*$ | Rolling radius of the (external ǀ internal) wheel to the curve including the displacement due to the yaw angle | m |
| $C_{11}\|C_{22}\|C$ | Longitudinal ǀ lateral ǀ vertical Kalker's coefficient | ∅ | $r_o$ | Nominal rolling radius | m |
| $C'_{11}\|C'_{22}$ | Kalker's coefficient (longitudinal ǀlateral) corrected according to non-dimensional slip components | ∅ | $r_p$ | Wheel radius measured until the flange contact patch | m |

| | | Unit (SI) | | | Unit (SI) |
|---|---|---|---|---|---|
| $C_{23}\mid C_{32}$ | Kalker's coefficients on $y_c z_c$ plane | ∅ | $r_{rr}$ | Real rolling radius | m |
| $D$ | Nominal wheel diameter | m⁻² | $r_H$ | Vertical Hertz's coefficient | ∅ |
| $e$ | Total bogie span (measured from its leading to its leading wheelset) | m⁻ | $R$ | Curve radius (measured from its center to the track axis) | m |
| $E$ | Equivalent Young's modulus of the materials in contact | m | $R_{x_1}$ | Rail lateral radius | m |
| $E_1\mid E_2$ | Young's modulus of the rail ⎸ wheel | m | $R_{x_2}$ | Wheel lateral radius | m |
| $F$ | Magnitude of tangential force vector | | $R_{y_1}$ | Rail longitudinal radius | m |
| $F_f$ | Braking force | Pa | $R_{y_2}$ | Longitudinal wheel radius | m |
| $F_t$ | Traction force | Pa | $s$ | Magnitude of non-dimensional slip vector | ∅ |
| $F_x\mid F_y$ | Longitudinal ⎸lateral tangential force | m | $s_x\mid s_y$ | Longitudinal⎸ lateral non-dimensional slip | ∅ |
| $F_x'\mid F_y'$ | Longitudinal ⎸lateral tangential force translated to the reference frame $\bar{u}\bar{v}\bar{w}$ | N | $s_C$ | Magnitude of non-dimensional slip corrected with the spin contribution | ∅ |
| $F_{y,C}$ | Lateral tangential force (lateral force) corrected with the spin contribution | N | $s_{y,C}$ | Lateral non-dimensional slip corrected with the spin contribution | ∅ |
| $F_{y,S}$ | Increase in lateral force due to spin | N | $T\gamma/A_c$ | Wear index for the USFD law | N · m⁻² |
| $F_{máx,RCF}$ | Maximum tangential force before rolling contact fatigue appears | N | $u_f$ | Coordinate in the $\bar{u}$ axis of the wheel contact area, in the reference frame $\bar{u}\bar{v}\bar{w}$ | m |
| $FI_{surf}$ | Fatigue index | N | $u_{fl}$ | Coordinate in the $\bar{u}$ axis of the flange outer part, in the frame $\bar{u}\bar{v}\bar{w}$ | m |
| $g$ | Gravity acceleration | N | $v_f$ | Coordinate in the $\bar{v}$ axis of the wheel contact area, in the frame $\bar{u}\bar{v}\bar{w}$ | m |
| $G$ | Equivalent shear modulus of the materials in contact | N | $v_{fl}$ | Coordinate in the $\bar{v}$ axis of the flange outer part, in the frame $\bar{u}\bar{v}\bar{w}$ | m |
| $G_1\mid G_2$ | Shear module of the rail ⎸ wheel | N | $v_x\mid v_y$ | Longitudinal⎸ lateral creepage | ∅ |
| $h_r$ | Real cant of the railway line | ∅ | $V$ | Vehicle speed | m · s⁻¹ |
| $H_{CdG}$ | Center of gravity of $\lambda_{eje}$ height over the rolling plane | m · s⁻² | $V_f\mid V_i$ | Final ⎸initial vehicle speed | m · s⁻¹ |
| $H_{tara}$ | Center of gravity of $\lambda_{tara}$ height over the rolling plane | Pa | $w_x\mid w_y$ | Longitudinal⎸ lateral slip speed | m · s⁻¹ |
| $H_u$ | Center of gravity of $\lambda_u$ height over the rolling plane | Pa | $R,USFD$ | Wear rate (USFD law) | kg · m⁻¹ · m⁻² |
| $H_{USFD}$ | Total wheel wear depth (USFD law) | m | $y$ | Wheelset uncentering | m |
| $i$ | Railway line gradient / slope | m | $y^*$ | Total wheelset uncentering | m |
| $J$ | Track gauge | m | $y_{lim}^*$ | Available play for the bogie leading wheelset when it uncenters towards the outside of a curve | m |
| $k$ | Wheel semi-conicity or inclination | m | $y_{lim,diag}^*$ | Available play for the bogie trailing wheelset when it uncenters towards the inside of a curve | m |
| $k_A\mid k_S$ | Reduction coefficient for the initial slope of the traction curve at the stick ⎸ slip region | m | $\dot{y}$ | Wheelset uncentering rate | m · s⁻¹ |
| $K_M$ | Auxiliary coefficient for the calculation of $F_{y,S}$ | ‰ | $\dot{y}^*$ | Total wheelset uncentering rate | m · s⁻¹ |
| $m_H$ | Longitudinal Hertz's coefficient | kg · m² | $Z_w$ | Number of wheels on the bogie | ∅ |
| | Spin torque | N | | | |

**Table A2**. Greek-symbol abbreviations.

| Abbreviation | Definition | Unit (SI) | Abbreviation | Definition | Unit (SI) |
|---|---|---|---|---|---|
| $\alpha_{fn}$ | Fraction of the force normal to the wheel falling on the flange contact patch | ∅ | $\mu_o$ | Initial friction coefficient or maximum (null slip speed) | ∅ |
| $\beta_{rp}$ | Gradient angle | rad | $\nu$ | Equivalent Poisson's ratio of the materials in contact | ∅ |
| $\gamma_o$ | Wheel contact angle | rad | $\nu_1\mid \nu_2$ | Poisson's ratio of the rail ⎸ wheel | ∅ |
| $\delta_o$ | Maximum indentation between the two bodies in contact | m | $\xi$ | Gauge widening (at tight curves) | m |

| | | | | | |
|---|---|---|---|---|---|
| $\delta_P$ | Auxiliary coefficient for the obtention of coefficient $K_M$ | $\emptyset$ | $\rho$ | Density of the wheel material | $kg \cdot m^-$ |
| $\varepsilon$ | Tangential stress gradient at the stick region | $\emptyset$ | $\varsigma$ | Longitudinal displacement angle of the contact patch | rad |
| $\varepsilon_S$ | Tangential stress gradient at the stick region for the pure spin case | $\emptyset$ | $\tau_{lím}$ | Tangential yield stress of the wheel material | Pa |
| $\eta$ | Play between the flange and the rail | m | | Tilt angle | rad |
| $\theta$ | Hertz's angle | rad | $\dot{\Phi}$ | Variation angle of tilt angle | $rad \cdot s^{-1}$ |
| $\vartheta_r$ | Real cant angle | rad | | Spin (rotational creepage) | $rad \cdot m^{-1}$ |
| $\lambda_{eje}$ | Axle load | kg | $\psi$ | Yaw angle | rad |
| $\lambda_{tara}$ | Vehicle tare | kg | $\dot{\psi}$ | Variation rate of yaw angle | $rad \cdot s^{-1}$ |
| $\lambda_u$ | Payload transported by the vehicle | kg | $\omega'$ | Angular slip speed when braking per unit length | $rad \cdot s^{-1} \cdot m^{-1}$ |
| $\mu$ | Dynamic friction coefficient (or adhesion coefficient) | $\emptyset$ | | | |

**Table A3**. Input values common to the three scenarios (920, 680 and 355-mm wheels).

| Variable | Value | Variable | Value | Variable | Value |
|---|---|---|---|---|---|
| $A_f$ ($\emptyset$) | 0.400 | $k\ (flange)$ ($\emptyset$) | 1.235 – 2.747 | $\gamma_o\ (tread)$ (º) | 1.432 |
| $B_f$ (s/m) | 0.600 | $k_A$ ($\emptyset$) | 1 | $\gamma_o\ (tread')$ (º) | 1.432 |
| $e$ (m) | 1.800 | $k_S$ ($\emptyset$) | 0.400 | $\gamma_o\ (P)$ (º) | 51 – 70 |
| $E_1$ (Pa) | $2.100 \cdot 10^{11}$ | $R_{x_1}\ (tread)$ (m) | $300 \cdot 10^-$ | $\eta$ (m) | 0.007 |
| $E_2$ (Pa) | $2.100 \cdot 10^{11}$ | $R_{x_1}(tread')$ (m) | $80 \cdot 10^-$ | $\lambda_{tara}$ (kg) | 20,000 |
| $g$ (m·s$^{-2}$) | 9.810 | $R_{x_1}(flange)$ (m) | $13 \cdot 10^-$ | $\mu$ ($\emptyset$) | 0,400 |
| $G_1$ (Pa) | $81.712 \cdot 10^9$ | $R_{x_2}\ (tread)$ (m) | $5 \cdot 10^7$ | $\mu_o$ ($\emptyset$) | 0.550 |
| $G_2$ (Pa) | $81.712 \cdot 10^9$ | $R_{x_2}\ (tread')$ (m) | $5 \cdot 10^7$ | $\nu_1$ ($\emptyset$) | 0.285 |
| $H_{tara}$ (m) | 0.512 | $R_{x_2}\ (flange)$ (m) | $(13\ or\ 20) \cdot 10^-$ | $\nu_2$ ($\emptyset$) | 0.285 |
| $H_{CdG}$ (m) | 1.573 | $n_{dec}$ ($\emptyset$) | 0 | $\rho$ (kg·m$^{-3}$) | 7,850 |
| $J$ (m) | 1.668 | $o$ (m) | 0.075 | $\tau_{lím}$ (Pa) | $3.120 \cdot 10^8$ |
| $k\ (tread)$ ($\emptyset$) | 0.025 | $w_w$ (m) | 0.140 | | |
| $k\ (tread')$ ($\emptyset$) | 0.025 | $\alpha_{fn}$ ($\emptyset$) | 0.750 | | |

**Notes:** (1) Tread' is the tread of the wheel opposed to the wheel experiencing flange – rail contact. (2) Some values are expressed as ranges since flange – rail contact geometry varies at every contact. (3) $5 \cdot 10^7$ means that the value tends to infinity ($\infty$ is not accepted on EES).

**Table A4**. Specific input values for each of the three scenarios.

| Variable | Value for 920-mm wheels scenario | Value for 680-mm wheels scenario | Value for 355-mm wheels scenario |
|---|---|---|---|
| $D$ (m) | 0.920 | 0.680 | 0.355 |
| $n_{ejes}$ ($\emptyset$) | 4 | 4 | 8 |
| $r_p$ (m) | 0.467 – 0.475 | 0.347 – 0.355 | 0.185 – 0.193 |
| $\lambda_{eje}$ (kg) | 18,784 | 15,325 | 6,996 |